




# Sliding Mode Control for Inverse Response Systems: A Trajectory Tracking Study

Gabriel Gómez-Guerra<sup>1,2</sup><sup>a</sup>, Sebastián Insuasti<sup>1,2</sup><sup>b</sup> and Oscar Camacho<sup>1</sup><sup>c</sup>

<sup>1</sup>*Colegio de Ciencias e Ingenierías "El Politécnico", Universidad San Francisco de Quito USFQ, Quito, Ecuador*

<sup>2</sup>*Instituto de Energía y Materiales, Universidad San Francisco de Quito USFQ, Quito, Ecuador*

**Keywords:** Inverse Response, Trajectory Tracking, Dynamic Sliding Mode Control, Continuous-Stirred Tank Reactor, TCLab.

**Abstract:** This paper introduces and compares three control strategies for systems exhibiting inverse response with variable reference tracking: Dynamic Sliding Mode Control (DSMC), Sliding Mode Control (SMC), and Proportional-Integral-Derivative (PID) control. These controllers were tested in two cases: using simulations in a nonlinear isothermal Continuous-Stirred Tank Reactor (CSTR) and in a modified Temperature Control Lab (TCLab). The results, both simulations and experimental, show that the DSMC consistently outperforms both the SMC and the PID controllers, delivering superior tracking performance in controlling the inverse response behavior when the reference is variable.

## 1 INTRODUCTION


Inverse response systems, also referred to as non-minimum phase systems, exhibit an initial reaction opposite to the desired steady-state outcome when subjected to a step input. This behavior poses challenges in control system design, often leading to issues like overshoot, extended settling times, and reduced stability margins. Inverse response systems are commonly encountered in various industrial applications, including chemical reactors, distillation columns, and certain mechanical systems (Liptak et al., 2018).


Controlling this process is challenging (Ogunnaike and Ray, 1994). Various methods have been employed, including classical control (Liptak et al., 2018), Smith predictor-based approaches (Alfaro and Vilanova, 2012), adaptive control (Chen, 2001), intelligent control (Estrada, 2021), as well as sliding mode control (Camacho et al., 1999; Rojas et al., 2005; Espín et al., 2023).


Implementing classical PID controllers for inverse response systems requires careful tuning, as these processes can cause stability issues. The derivative control term is often not beneficial for stability. High

controller gain may lead to runaway effects, while low gain results in sluggish control loops, where increasing speed compromises stability (Ogunnaike and Ray, 1994).

Alternatively, sliding mode control (SMC) is a non-linear approach widely utilized in both theoretical and practical applications within industrial processes (Camacho et al., 1997; Utkin et al., 2020). Its popularity comes from its ability to handle uncertain system conditions and maintain robust control performance in the face of disturbances (Furat and Eker, 2012; Sardella et al., 2021; Mehta and Bandyopadhyay, 2021; Gambhire et al., 2021). In real-world scenarios, the appeal of the SMC technique lies in its proficiency in managing highly nonlinear processes, systems with time delays, changing operating conditions, variations in model parameters, disturbances, and uncertainties (Utkin et al., 2020). The SMC strategy defines a surface or manifold that guides the process output to its desired final value. Specifically, a sliding surface and its time derivatives are selected based on performance requirements, with  $S(t)$  chosen so that system dynamics are constrained to this sliding mode surface. Selecting an appropriate sliding mode surface  $S(t)$  effectively reduces the control parameters necessary for optimal global control system performance (Utkin et al., 2020). The structure of an SMC scheme is variable and adapts based on

<sup>a</sup> <https://orcid.org/0009-0008-8002-0277>

<sup>b</sup> <https://orcid.org/0009-0001-6958-795X>

<sup>c</sup> <https://orcid.org/0000-0001-8827-5938>

the current system states to the selected sliding surface; however, high-frequency oscillatory responses, known as chattering, may arise when tracking certain equilibrium points (Camacho and Smith, 2000). The chattering effect can lead to reduced control performance, increased actuator wear, unnecessary energy consumption, and system instability.

The dynamic sliding mode control (DSMC) strategy modifies the traditional sliding mode control (SMC) switching function to create a new function that diminishes the chattering effect. This function involves either the first or a higher-order derivative of the control input, allowing the shifting of discontinuous components to these derivatives (Sira et al., 1994; Utkin et al., 2020). Recently, the synthesis of DSMC designs has attracted interest (Proaño et al., 2017; Gambhire et al., 2021; Espín et al., 2023), as adding extra dynamics to a sliding surface addresses practical challenges.

Despite the extensive literature on SMC, it is worth noting that SMC has not traditionally been applied to control non-linear chemical processes that exhibit an inverse response (Castellanos-Cárdenas et al., 2022; Camacho et al., 1999; Rojas et al., 2005; Espín et al., 2023; Gómez et al., 2023). In addition, none of these studies have addressed tracking variable references. To the best of our knowledge, this marks the first attempt to employ SMC for chemical processes with inverse response and variable reference tracking.

This paper compares and evaluates sliding mode control techniques that aim to improve the performance of variable reference tracking. Several studies have shown that the implementation of variable temperature profiles (Ahn et al., 2009; Pataro et al., 2023; Sardella et al., 2021) during the operation of processes, such as batch reactors, can significantly enhance their overall efficiency. This optimization is achieved by carefully controlling the thermal environment to maximize the release of fermentable sugars. By adjusting the temperature at different stages of the reaction, the breakdown of complex biomass components into simpler fermentable sugars is more effective, leading to improved yields and reduced processing times. Therefore, increasing the efficiency of the fermentation process also contributes to energy savings and cost reduction in biofuel production, as demonstrated in (Vegi and Shastri, 2017). Although most existing research focuses on regulation or step function tracking, this study emphasizes the importance of dynamic reference tracking for improving process response and performance.

The paper is divided as follows: in Section two, some fundamentals are described; Section three shows the designed controllers; in Section four, the

results by simulations are presented; and finally, the conclusion.

## 2 FUNDAMENTALS

This Section introduces several concepts that support the design of the control strategies used in this work.

### 2.1 Inverse Response System

An inverse response system is characterized by a transfer function with zeros in the right half of the plane, causing the initial slope to oppose the final steady-state value. An inverse response system can be modeled by two first-order systems that form the transfer function described in (1). This model has been proven to accurately replicate the behavior of the real plant (Camacho et al., 2020).

$$G(s) = \frac{K(-\eta s + 1)}{(\tau_1 s + 1)(\tau_2 s + 1)} \quad (1)$$

### 2.2 Iinoya-Alpeter Compensator

The controller method aims to address the challenges of non-minimum phase behavior, also known as the inverse response, by employing the Iinoya-Alpeter compensator. This compensator uses an Internal Model Controller to transform the system into a minimum phase system. Inverse response systems are non-minimum phase due to a zero in the right-half plane, which introduces instability and limits practical closed-loop performance by restricting controller bandwidth. This leads to delays in plant response and lower product quality. The Iinoya-Alpeter compensator mitigates these adverse effects by introducing an internal transfer function into the feedback loop, effectively neutralizing the impact of the zero of the right half-plane. The block diagram of the Iinoya-Alpeter compensator is shown in Figure 1.

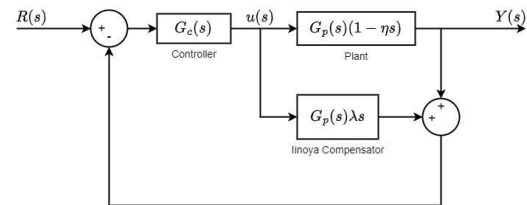


Figure 1: Iinoya-Alpeter compensator block diagram.

Where  $G_p(s)$  represents the plant transfer function without the right half-plane zero, and  $\lambda$  is a parameter, optimized to the value  $2\eta$ , to compensate for the right-half-plane zero (Ogunnaike and Ray, 1994). With this

control scheme, the controller receives as input a minimum phase system given by (2).

$$G(s) = \frac{K(\eta s + 1)}{(\tau_1 s + 1)(\tau_2 s + 1)} \quad (2)$$

### 2.3 Inverse Response Systems Identification

There are several methods for inverse response systems. In this paper, the Alfaro and Balaguer identification method (Balaguer et al., 2011) is used to model an inverse response system as a second-order inverse response model. The procedure can be found in a detailed way in (Balaguer et al., 2011). The resulting analysis produces a transfer function as shown in (1).

Another way is to consider a First-Order Plus Dead Time (FOPDT) system, in which, using a Taylor approximation, the dead time term is considered as the right zero term since it does not account for the inverse response term directly. A FOPDT system consists of a pole formed by the systems time constant,  $\tau$ , a proportional gain,  $K$ , and a time delay,  $t_0$ , as represented by the transfer function in (3).

$$G(s) = \frac{K}{\tau s + 1} e^{-t_0 s} \quad (3)$$

In (Alfaro, 2001) can be found different approaches for identification.

## 3 CONTROL LAWS

This section discusses the control laws applied in this work: first, a PID controller, followed by a Sliding Mode Control, and finally a Dynamical Sliding Mode Controller.

### 3.1 PID Controller

The first control law proposed is a PID controller. For this scheme, the system is modeled as an inverse response system described in section 2.3.

#### 3.1.1 Controller Design

For this study, a proportional-integral-derivative controller was chosen. The action of the PID controller is calculated as (4).

$$u(t) = K_P \left( e(t) + T_d \frac{de(t)}{dt} + \frac{1}{T_i} \int e(t) dt \right) \quad (4)$$

Where  $K_P$ ,  $T_d$  and  $T_i$  represent the proportional, derivative and integral parameters of the controller.

The parameter tuning equations are derived from (Camacho et al., 2020). The proportional gain of the controller was calculated as (5).

$$K_P = \frac{1}{K} \left( \frac{\tau_1 + \tau_2 + \frac{\eta t_0}{\tau_c + \eta + t_0}}{\tau_c + \eta + t_0} \right) \quad (5)$$

Where  $\tau_c$  is a tuning parameter selected as (6).

$$\frac{\tau_c}{t_0} > 0.8 \text{ and } \tau_c > 0.1\tau \quad (6)$$

Similarly, the integral gain is calculated as (7).

$$T_i = \tau_1 + \tau_2 + \frac{\eta t_0}{\tau_c + \eta + t_0} \quad (7)$$

Finally, the derivative gain is calculated as (8).

$$T_d = \frac{\eta t_0}{\tau_c + \eta + t_0} + \frac{\tau_1 \tau_2}{\tau_1 + \tau_2 + \frac{\eta t_0}{\tau_c + \eta + t_0}} \quad (8)$$

### 3.2 SMC Controller Design

The SMC algorithm consists of two main stages: the reaching phase and the sliding mode phase. During the reaching phase, the state of the system is driven towards a user-defined surface, while in the sliding mode phase, the dynamics of the system are constrained to follow the dynamics of the surface, making the system robust to parameter variations and disturbances (Camacho and Smith, 2000; Salinas et al., 2018). Known for its robustness and insensitivity to parameter variations, the conventional SMC theory applied to inverse response systems can lead to instability, as noted in (Camacho et al., 1999; Rojas et al., 2005; Castellanos-Cárdenas et al., 2022).

One way to apply conventional SMC to this kind of system is to model the system as a First-Order Plus Dead Time (FOPDT). The controller design follows the method described by (Camacho et al., 1999), which uses a proportional-integral-derivative equation as the surface to ensure reliability and robustness. Applying this procedure to a FOPDT system yields the result shown in (9).

$$u_c(t) = \frac{t_0 \tau}{K} \left[ \left( \frac{1}{t_0 \tau} - \lambda_0 \right) y(t) + \frac{d^2 r(t)}{dt^2} + \lambda_1 \frac{dr(t)}{dt} + \lambda_0 r(t) \right] + K_D \frac{S(t)}{|S(t)| + \delta} \quad (9)$$

Where,  $r(t)$  represents the reference trajectory to be followed, and  $y(t)$  is the system output. The parameters  $\lambda_1$ ,  $\lambda_0$ ,  $K_D$ , and  $\delta$  are chosen to ensure controller stability. Additionally,  $S(t)$  denotes the PID surface equation, which in this case is given by (10).

$$S(t) = \frac{de(t)}{dt} + \lambda_1 e(t) + \lambda_0 \int_0^t e(t) dt \quad (10)$$

To eliminate the output derivative from the controller action,  $\lambda_1$  should be set as specified in (11).

$$\lambda_1 = \frac{t_0 + \tau}{t_0 \tau} \quad (11)$$

Finally,  $\lambda_0$  was tuned taking into account the constraint set in (12).

$$0 < \lambda_0 < \min \left[ \frac{\lambda_1}{\eta}, \frac{\lambda_1^2}{4} \right] \quad (12)$$

The reaching controller parameters  $K_D$  and  $\delta$  were manually adjusted.

### 3.3 Dynamical Sliding Mode Controller Design

The design begins with the system model, which includes its inverse response as shown in (1). To mitigate the effect of the inverse response, Iinoya's compensator was applied with  $\lambda = 2\eta$ , transforming the system into a minimum phase system as described in (2).

Subsequently, the system was expressed as a differential equation in its "normal form" by applying the inverse Laplace transform, as illustrated in (13).

$$\begin{aligned} \frac{d^2 y^*(t)}{dt^2} = & -\frac{(\tau_1 + \tau_2)}{(\tau_1 \tau_2)} \frac{dy^*(t)}{dt} - \frac{y^*(t)}{(\tau_1 \tau_2)} \\ & + \frac{K\eta}{(\tau_1 \tau_2)} \frac{du(t)}{dt} + \frac{K}{(\tau_1 \tau_2)} u(t) \end{aligned} \quad (13)$$

From (13) the controller action derivative was isolated as in (14).

$$\begin{aligned} \frac{K\eta}{(\tau_1 \tau_2)} \frac{du(t)}{dt} = & \frac{d^2 y^*(t)}{dt^2} + \frac{(\tau_1 + \tau_2)}{(\tau_1 \tau_2)} \frac{dy^*(t)}{dt} \\ & + \frac{y^*(t)}{(\tau_1 \tau_2)} - \frac{K}{(\tau_1 \tau_2)} u(t) \end{aligned} \quad (14)$$

A sliding surface needed to be chosen to define the system's dynamics. Given that the process has two poles and a stationary error, a proportional-integral-derivative (PID) surface was selected, as shown in (15).

$$S(t) = 2\alpha e(t) + \alpha^2 \int_0^t e(t) dt + \frac{de(t)}{dt} \quad (15)$$

To ensure that the process remains on the surface, (15) was derived and set to 0 as presented in (16).

$$\frac{dS(t)}{dt} = \alpha^2 e(t) + 2\alpha \frac{de(t)}{dt} + \frac{d^2 e(t)}{dt^2} = 0 \quad (16)$$

The error definition,  $e(t) = r(t) - y(t)$ , was substituted in (16), and the resulting expression was incorporated into the controller algorithm. This substitution simplifies the output derivatives and yields the controller action as reported in (17).

$$\begin{aligned} \frac{K\eta}{(\tau_1 \tau_2)} \frac{du(t)}{dt} = & \left( \frac{(\tau_1 + \tau_2)}{(\tau_1 \tau_2)} - 2\alpha \right) \frac{dy^*(t)}{dt} \\ & + \frac{y^*(t)}{(\tau_1 \tau_2)} - \frac{K}{(\tau_1 \tau_2)} u(t) + \alpha^2 e(t) + \alpha \frac{dr(t)}{dt} + \frac{d^2 r(t)}{dt^2} \end{aligned} \quad (17)$$

Setting  $\alpha$  as in (18), the output derivative was eliminated.

$$\alpha = \frac{(\tau_1 + \tau_2)}{2\tau_1 \tau_2} \quad (18)$$

Additionally, a reaching controller component, including parameters  $K_D$  and  $\delta$ , was designed. As with the SMC, these parameters were manually tuned.

By replacing these considerations with (17) and isolating the controller action derivative, the DSMC control law was obtained as (19).

$$\begin{aligned} \frac{du(t)}{dt} = & \frac{y^*(t)}{K\eta} + \frac{(\tau_1 + \tau_2)^2}{(4\tau_1 \tau_2 K\eta)} e(t) + \frac{(\tau_1 + \tau_2)}{K\eta} \frac{dr(t)}{dt} \\ & + \frac{\tau_1 \tau_2}{K\eta} \frac{d^2 r(t)}{dt^2} - \frac{u(t)}{\eta} + K_D \frac{S(t)}{|S(t)| + \delta} \end{aligned} \quad (19)$$

## 4 RESULTS AND DISCUSSION

In this section, the three controller approaches were tested and evaluated. Two systems are used to evaluate the controller performance: a continuous-stirred tank reactor (CSTR) and a temperature control laboratory (TCLab). The CSTR, a non-linear system previously characterized and tested in (Balaguer et al., 2011), will be simulated using its physical model as presented below. The proposed control laws and system simulations will be conducted in Simulink. The TCLab, shown in Figure 8, is a laboratory equipment used for real-time temperature control experiments. It features two controllable heating resistors and is operated via a Simulink interface connected through a USB serial communication port.

### 4.1 Continuous-Stirred Tank Reactor (CSTR)

The chemical reactor simulated in this paper is an isothermal Continuous-Stirred Tank Reactor (CSTR) that can exhibit inverse response due to a Van der

Vusse reaction. While this system has been analyzed in previous works (Balaguer et al., 2011), this paper introduces a novel control law for variable reference tracking, which, to the best of our knowledge, has not been proposed before. Figure 2 shows the CSTR system used to validate the proposed control laws, as adapted from (Balaguer et al., 2011).

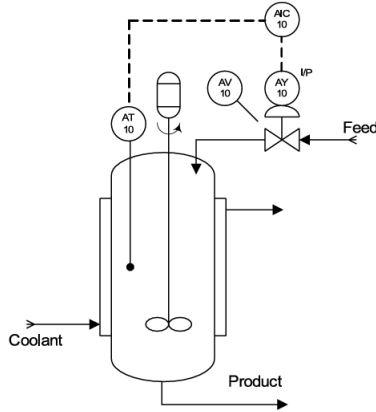


Figure 2: CSTR isothermal reactor (Balaguer et al., 2011).

The variables of interest are the output chemical concentration,  $C_B$ , which is the controlled variable, and the flow through the reactor,  $F_r$ , which is the manipulated variable.

#### 4.1.1 Nonlinear Model

According to (Balaguer et al., 2011), the CSTR operates with an initial concentration of the first chemical,  $C_{A0}$ , of  $2.9175 \text{ mol/l}$  and an initial concentration of the output chemical,  $C_{B0}$ , of  $1.1 \text{ mol/l}$ . Due to the system's non-linearity, reference changes should be within a  $\pm 10\%$  range.

For the examination of system dynamics, the subsequent assumptions were taken into account:

- Heat and density capacities of the reactants are constant
- The heat loss in coolant jacket is considered negligible
- The reaction heat and volume remain constant
- The reaction and reacted material are uniformly mixed

The mathematical model of the CSTR is obtained based on exothermic reactions according to (Alfaro and Vilanova, 2012; Balaguer et al., 2011). A process reaction in a CSTR can be described as follows:



Table 1: Operation values of the continuous stirred reactor tank.

Model parameters	Value
$k_1$	$\frac{5}{6} \text{ min}^{-1}$
$k_2$	$\frac{5}{3} \text{ min}^{-1}$
$k_3$	$\frac{1}{6} \text{ l} \cdot \text{mol}^{-1} \cdot \text{min}^{-1}$
$C_{Ai}$	$10 \text{ mol} \cdot \text{l}^{-1}$
$V$	$700 \text{ l}$
$C_{A0}$	$2.9175 \text{ mol} \cdot \text{l}^{-1}$
$C_{B0}$	$1.1 \text{ mol} \cdot \text{l}^{-1}$
$u_{0\%}$	$60\%$

Where  $A \xrightarrow{K_1} B$  stands for an exothermic reaction. From a mass balance on reactants A and B, the system can be described as follows:

$$\frac{dC_A(t)}{dt} = \frac{F_r(t)}{V} [C_{Ai} - C_A(t)] - k_1 C_A(t) - k_3 C_A^2(t) \quad (22)$$

$$\frac{dC_B(t)}{dt} = -\frac{F_r(t)}{V} C_B(t) + k_1 C_A(t) = k_2 C_B(t) \quad (23)$$

For practical purposes, it should be considered that the control range of the concentration B is from 0 to  $1.5714 \text{ mol l}^{-1}$ ; the range of variation of the flow is from 0 to  $634.1719 \text{ l min}^{-1}$ . In addition, the transmitter signal  $y$ , process input  $u$ , and flow through the reactor  $F_r$  are presented in percentage.

The sensor-transmitter element takes the form:

$$y(t)\% = \left( \frac{100}{1.5714} \right) C_B(t) \quad (24)$$

The relation for the flow through the reactor as a function of the process input through the control valve is linear:

$$F_r(t) = \left( \frac{634.1719}{100} \right) u(t)\% \quad (25)$$

Variables of the mathematical model for the CSTR process are detailed as follows:

$F_r$ : flow through the reactor

$V$ : reactor volume that will remain constant during operation

$C_A$ : the concentration of A in the reactor ( $\text{mol l}^{-1}$ )

$C_B$ : the concentration of B in the reactor ( $\text{mol l}^{-1}$ )

$C_{A0}$ : the concentration of A in steady-state ( $\text{mol l}^{-1}$ )

$C_{B0}$ : the concentration of B in steady-state ( $\text{mol l}^{-1}$ )

$k_i (i = 1, 2, 3)$ : the reaction rate constants for the three reactions

$y(t)\%$ : transmitter signal

$u(t)\%$ : process input

Table 1 shows the steady-state conditions for each variable in the CSTR process.

#### 4.1.2 System Identification as an Inverse Response Model

The CSTR system was identified as a second-order inverse response system (Balaguer et al., 2011) to simplify the controller design. During the identification process, a 10% step input change was applied at time zero to the system. The transfer function of the identified CSTR model is given in equation (26).

$$G_{RI} = \frac{0.32(-0.356s + 1)}{(0.35s + 1)(0.483s + 1)} \quad (26)$$

Figure 3 illustrates the behavior of the CSTR system along with the model described by equation (26). The model accurately replicates the system's behavior, although there is a slight discrepancy in the concentration drop. Despite this minor deviation, the model error is not significant enough to impact the control law.

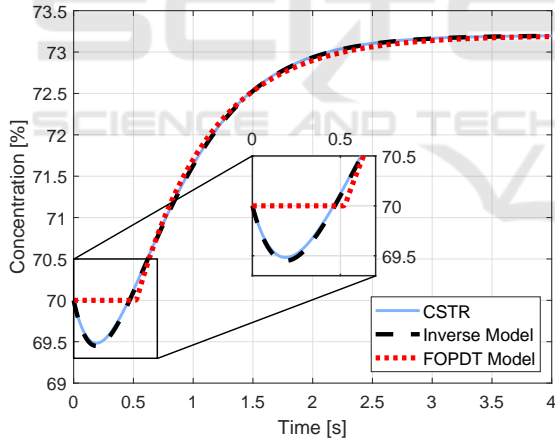


Figure 3: CSTR system identification.

#### 4.1.3 System Identification as a FOPDT Model

Similarly, the CSTR system was identified as a First-Order Plus Dead Time (FOPDT) model (Seborg et al., 2016). A step input with a 10% change was applied to the CSTR system for this identification. The resulting transfer function is provided in equation (27).

$$G_{TF} = \frac{0.32}{(0.625s + 1)} e^{-0.525s} \quad (27)$$

The model obtained is validated by comparing its behavior with the actual CSTR system, as shown in

Figure 3. The model accurately replicates the behavior of the CSTR system. The detailed graph shows that the model effectively omits the inverse response and exhibits only minimal error compared to the real system. This small modeling error is not significant enough to affect the control law.

#### 4.1.4 Tuning Parameters of Controllers

Furthermore, the three control laws were tuned according to the procedure outlined in Section 3. The tuning parameters used in this work are provided in Table 2 for both systems.

Table 2: Tuning parameters for the proposed control laws.

Controller	Parameter	CSTR	TCLab
PID	$K_P$	3.63	0.63
	$T_i$	0.99	234.81
	$T_d$	0.25	54.67
SMC	$\lambda_0$	3.07	$2.95E - 5$
	$\lambda_1$	3.50	0.0109
	$K_D$	9.68	2.176
	$\delta$	1	1
DSMC	$\alpha$	2.03	0.0103
	$K_D$	1217.8	5.44
	$\delta$	1	1

#### 4.1.5 Performance Indicators

Performance evaluation is performed using the Integral Squared Error (ISE), as defined in (28), and the Integral Squared Controller Output (ISCO), as shown in (29).

$$ISE = \int e(t)^2 dt \quad (28)$$

$$ISCO = \int u(t)^2 dt \quad (29)$$

where ISE quantifies performance by integrating squared error over time and ISCO measures control signal effort (Seborg et al., 2016; Liptak et al., 2018).

#### 4.1.6 Simulation Results

The CSTR system was tested with three control laws in two tests: one with a constant frequency variable reference and the other varying the reference oscillation frequency to evaluate the control bandwidth.

For the first two seconds of the constant frequency test, the reference was kept constant at 60% concentration. The remainder of the test was designed as described in Equation (30).

$$R_C(t) = 60 + 5 \cdot \sin(0.1(t - 2)) + 2.05(t - 2) \cdot \sin(0.4(t - 2)) \quad (30)$$

Figure 4 illustrates the behavior of the CSTR system with the three controllers for the reference described in (30).

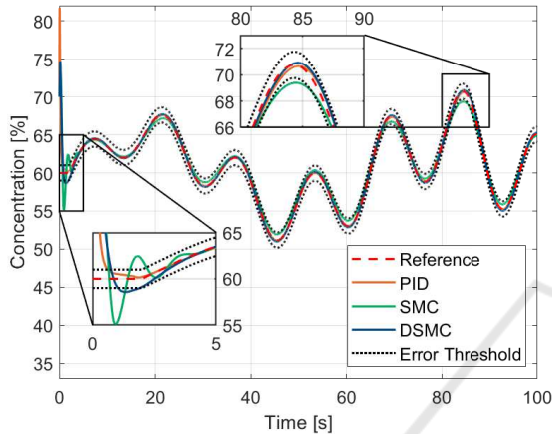


Figure 4: CSTR system: reference tracking at constant frequency results.

It is observed that the system initially exhibits strong oscillations around the reference. However, once it settles, all three controllers accurately follow the trajectory. However, during significant upward variations in the reference, the controllers struggle to keep up, particularly the SMC controller, as highlighted in detail in Figure 4. In contrast, Figure 5 presents the controller actions for this experiment.

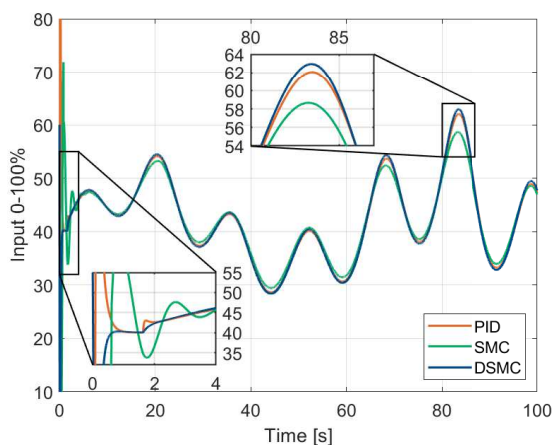


Figure 5: CSTR system: reference tracking at constant frequency controller action.

Initially, as shown in the first detail of Figure 5, all three controllers exhibit strong control actions. However, in the second detail, the control actions are insufficient to follow the designed reference.

To compare the performance of the controllers, an error threshold was established within a 2°C range around the reference (Figure 4). This threshold assesses the time each controller takes to reach and stay within this range, termed the settling time for variable reference. The calculated performance indicators are reported in Table 3

Table 3: CSTR system performance indicators.

PI	PID	SMC	DSMC
ISE	143.4	131.49	19.4
ISCO [ $\cdot 10^4$ ]	3.74	3.7	3.81
ts [s]	2.8	2.16	1.86

To better visualize the comparison between controllers, Figure 6 illustrates the normalized performance indicators.

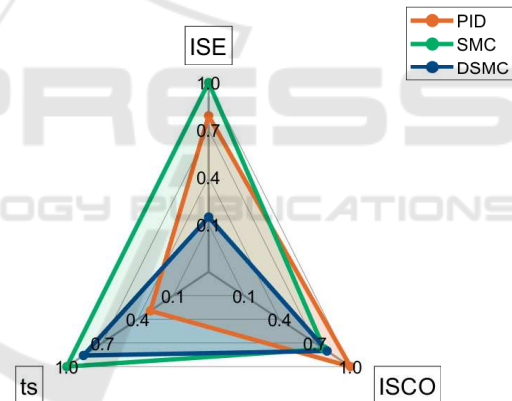


Figure 6: CSTR system: performance comparison.

The DSMC controller demonstrates superior performance compared to the other two control laws. However, it is noteworthy that the controller actions are quite similar across all three laws. The settling times for the controllers are also comparable. Despite this, the DSMC controller achieves a smaller error than the others. On the other hand, between the PID and SMC schemes, it is observed that the PID outperforms the SMC in every indicator except ISCO.

The second test on the CSTR system examined variable frequency reference tracking to determine the operating bandwidth. Typically, Bode diagrams analyze a control system's frequency response by comparing the controller's output with the system's output for stability and performance. However, this ap-

proach uses a variable reference as the open-loop input and compares it with the system's output to assess the system's tracking ability.

The primary objective of this analysis is to identify the reference frequency range in which the controller can operate optimally. To achieve this, the magnitude plot will be examined, as it provides a comparison of the ratio between the system's output and the variable frequency input reference, expressed in decibels (dB). This analysis is crucial for understanding the system's dynamic behavior and ensuring effective control across various operating conditions. Equation (31) shows how the magnitude plot of the BODE diagram was calculated. By establishing the appropriate frequency range, we can enhance the controller's performance and improve overall system stability.

$$|H(s)| = 20 \log_{10} \left| \frac{Y(s)}{R(s)} \right| \quad (31)$$

In this context,  $Y(s)$  represents the system output, while  $R(s)$  denotes the variable frequency reference. Consequently, the closer the magnitude approaches to 0dB, the closer the output will align with the reference.

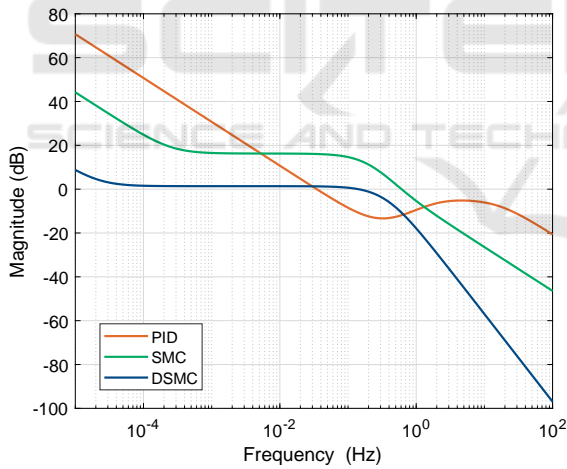


Figure 7: Magnitude bode diagram for variable frequency reference.

Figure 7 illustrates the relationship between the variable frequency reference and the system output.

The Bode diagram reveals that the DSMC controller exhibits a one-to-one correspondence between the reference and system output across frequencies ranging from 0.1 mHz to 0.1 Hz, indicating the highest performance and bandwidth. The SMC controller performs well within a bandwidth of 1 mHz to 50 mHz, with a nearly one-to-one correlation. In contrast, the PID controller shows the poorest performance.

The behavior of the PID controller does not exhibit a distinct range in which it operates optimally.

## 4.2 Temperature Control Lab

As previously mentioned, the TCLab is a laboratory device used for real-time temperature control experiments. It has been extensively characterized in the literature, demonstrating that the temperature system can be modeled as a First-Order Plus Dead Time (FOPDT) system (Rossiter et al., 2023; Park et al., 2020; Insuasti et al., 2022). To model the FOPDT system as an inverse response system, an inversion module is added in series with the temperature plant. This module is defined by a transfer function with a zero in the right-half plane and a pole, as given in (32).

$$G_I(s) = \frac{1 - \eta s}{\tau_1 s + 1} \quad (32)$$

Following the process described in (Gómez et al., 2023), the inversion module is designed to induce a temperature drop of approximately 5°C. Thus, the transfer function of the inversion module is given by (33).

$$G_I(s) = \frac{1 - 140s}{60s + 1} \quad (33)$$

With the addition of this inversion module, the temperature plant block diagram for the remainder of this paper is as shown in Figure 8.

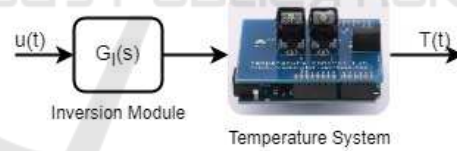


Figure 8: Temperature system block diagram.

Figure 9 illustrates the behavior of the temperature system with the inversion module. As mentioned, the initial temperature drop is approximately 5°C, for a step change of 20%.

### 4.2.1 System Identification as an Inverse Response Model

The system shown in Figure 8 is modeled as an inverse response system with the transfer function provided in (1). To identify the system, a step input with a 20% change was applied, following the method described in Section 2.3. The transfer function of the inverse temperature system is given in (34).

$$G_{TI} = \frac{0.86(-163s + 1)}{(156.8s + 1)(70.5s + 1)} \quad (34)$$



Figure 9 shows the behavior of both the real system and the identified model. The proposed model accurately replicates the behavior of the real system. However, since the physical system lacks a cooling mechanism, the actual temperature system takes longer to achieve the temperature drop compared to the model.

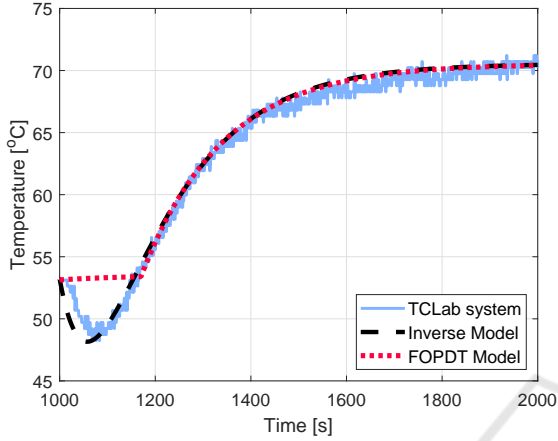


Figure 9: Temperature system identification.

#### 4.2.2 System Identification as a FOPDT Model

Following the procedure described in Section 2.3, the inverse temperature system is identified as a First-Order Plus Dead Time (FOPDT) model, as given in (3). For the identification process, a step input with a 20% change is applied to the system shown in Figure 8. The transfer function of the identified system is provided in equation (35).

$$G_{TF} = \frac{0.86}{(170.9s + 1)} e^{-199.96s} \quad (35)$$

The behavior of the identified FOPDT system is validated by comparing it with the real system, as shown in Figure 9. The model accurately captures the behavior of the system and eliminates the inverse response, confirming that it helps in the design of the SMC controller by removing the term of inverse response from the transfer function.

#### 4.2.3 Experimental Results

To assess the performance of the three control laws in the temperature system, a variable reference was designed. For the first 300 seconds of the experiment, the reference was kept constant at 50° C. After this period, the reference follows the equation given in (36). The frequency of the reference change is kept low to allow the system to cool naturally, due to the absence

of external cooling in the plant.

$$R_T(t) = 50 \cdot \sin\left(\frac{1}{500}(t - 300)\right) \quad (36)$$

Figure 10 illustrates the behavior of the system using the three proposed control laws for constant frequency reference tracking.

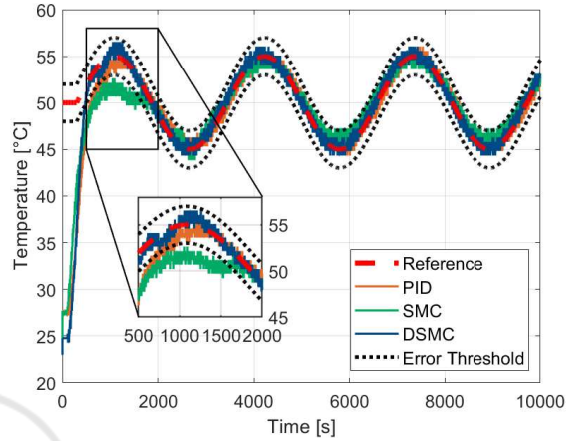


Figure 10: Temperature system: reference tracking test results.

The DSMC controller reaches the reference faster than the others, but all controllers track the reference effectively. Figure 11 shows the controller actions for each control law during the experiment.

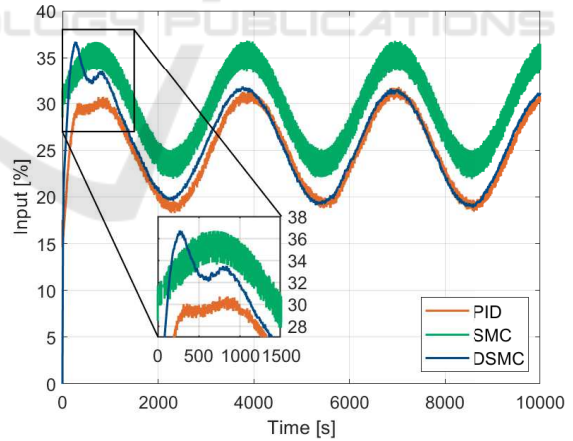


Figure 11: Temperature system: reference tracking controller action.

It is observed that the DSMC controller exhibits a stronger initial action to quickly catch up with the reference. However, the DSMC controller's action then stabilizes within a range of 20% to 32%. Similarly, the PID controller's action also settles within this range but takes longer to reach the temperature reference. In contrast, the SMC controller demonstrates a higher overall control action but is the slow-

est to respond to significant changes in the reference.

The performance indicators described in Section 4.1.5 were measured to compare the behavior of the three proposed control laws. Table 4 reports the results obtained.

The performance indicators measured during the experiment, including the ISE, ISCO, and settling time, are summarized in Table 4.

Table 4: Temperature system performance indicators.

PI	PID	SMC	DSMC
ISE [ $\cdot 10^5$ ]	2.66	2.08	0.2873
ISCO [ $\cdot 10^6$ ]	6.5	9.2	6.95
ts [s]	654	1620	488

Figure 12 presents the normalized performance indicators. The settling time was defined as described in Section 4.1.6.

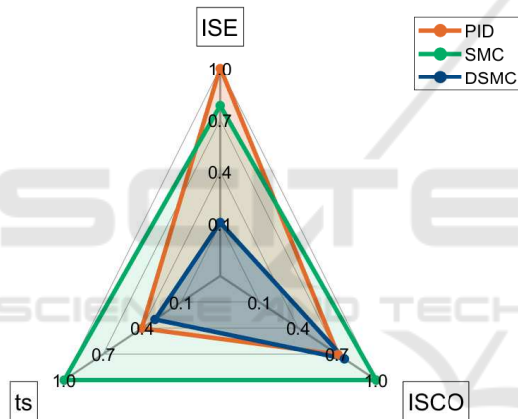


Figure 12: Temperature system: performance comparison.

Figure 12 shows the DSMC controller outperforms others with smaller error, smoother action, and faster tracking, while the SMC controller performs the worst with slower tracking, higher error, and higher action.

## 5 CONCLUSIONS

This study introduced and compared three control laws for systems with inverse response and variable references: a Dynamic Sliding Mode Controller (DSMC), a Sliding Mode Controller (SMC), and a PID controller. These control laws were tested on two different systems: a Continuous-Stirred Tank Reactor (CSTR) and a software-modified Temperature Control Lab (TCLab). The simulations and experimen-

tal results demonstrate that all three control laws can track a variable reference, but the DSMC controller outperforms both the SMC and the PID controllers.

Future research could further investigate the robustness of the Dynamic Sliding Mode Controller (DSMC) by testing it in more complex environments, including disturbances and systems with higher time delays. Additionally, implementing these control strategies on hardware systems beyond the TCLab, such as industrial-scale processes or robotics, would help validate their practicality and effectiveness in real world applications. Extending the analysis to multivariable systems could also offer deeper insights into the scalability and adaptability of the DSMC approach.

## ACKNOWLEDGEMENTS

This work was supported by the Universidad San Francisco de Quito's Poli-Grants Program, Grant 24280.

## REFERENCES

- Ahn, H.-S., Bhambhani, V., and Chen, Y. (2009). Fractional-order integral and derivative controller for temperature profile tracking. *Sadhana*, 34:833–850.
- Alfaro, V. (2001). Identificación de procesos sobreamortiguados utilizando técnicas de lazo cerrado. *Ingeniería*, 11:27–40.
- Alfaro, V. M. and Vilanova, R. (2012). Two-degree-of-freedom proportional integral control of inverse response second-order processes. In *2012 16th International Conference on System Theory, Control and Computing (ICSTCC)*, pages 1–6. IEEE.
- Balaguer, P., Alfaro, V., and Arrieta, O. (2011). Second order inverse response process identification from transient step response. *ISA Transactions*, 50(2):231–238.
- Camacho, O., Rojas, R., and García, W. (1999). Variable structure control applied to chemical processes with inverse response. *ISA Transactions*, 38(1):55–72.
- Camacho, O., Rosales, A., and Rivas, F. (2020). *Control de Procesos*. Escuela Politécnica Nacional, 1 edition.
- Camacho, O. and Smith, C. A. (2000). Sliding mode control: an approach to regulate nonlinear chemical processes. *ISA Transactions*, 39(2):205–218.
- Camacho, O. E., Smith, C., and Chacón, E. (1997). Toward an implementation of sliding mode control to chemical processes. In *ISIE'97 Proceeding of the IEEE International Symposium on Industrial Electronics*, pages 1101–1105. IEEE.
- Castellanos-Cárdenas, D., Hernandez, F., Vasquez, R., Posada, N., and Camacho, O. (2022). A new sliding mode control tuning approach for second-order

- inverse-response plus variable dead time processes. *Journal of Process Control*, 115:77–88.
- Chen, C.-T. (2001). Direct adaptive control of chemical process systems. *Industrial & engineering chemistry research*, 40(19):4121–4140.
- Espín, J., Estrada, S., Benítez, D., and Camacho, O. (2023). A hybrid sliding mode controller approach for level control in the nuclear power plant steam generators. *Alexandria Engineering Journal*, 64:627–644.
- Estrada, M. (2021). *Toward the Control of Non-Linear, Non-Minimum Phase Systems via Feedback Linearization and Reinforcement Learning*. PhD thesis, University of California Berkeley, CA, USA.
- Furat, M. and Eker, İ. (2012). Experimental evaluation of sliding-mode control techniques. *Çukurova Üniversitesi Mühendislik-Mimarlık Fakültesi Dergisi*, 27(1):23–37.
- Gambhire, S., Kishore, D. R., Londhe, P., and Pawar, S. (2021). Review of sliding mode based control techniques for control system applications. *International Journal of dynamics and control*, 9(1):363–378.
- Gómez, G., Fabara, J., Herrera, M., and Camacho, O. (2023). Control of processes with inverse response and long-dead-time: An experimental evaluation. In *2023 IEEE Seventh Ecuador Technical Chapters Meeting (ECTM)*, pages 1–6.
- Insuasti, S., Paredes, J. L., and Camacho, O. (2022). Controllers and compensators design for undergraduate control students: Testing with tclab arduino kit. In *2022 IEEE Sixth Ecuador Technical Chapters Meeting (ETCM)*, pages 1–6.
- Liptak, B. G., Piovoso, M. J., Shinsky, F. G., Eren, H., Tothorow, G. K., Jamison, J. E., Morgan, D., Hertanu, H. I., Marszal, E. M., Berge, J., et al. (2018). *Instrument engineers' handbook, volume two: Process control and optimization*. CRC press.
- Mehta, A. and Bandyopadhyay, B. (2021). Emerging trends in sliding mode control. *Studies in Systems, Decision and Control*, 318.
- Ogunnaike, B. and Ray, W. (1994). *Process Dynamics, Modeling, and Control*. Topics in Chemical Engineering - Oxford University Press. Oxford University Press.
- Park, J., Martin, R. A., Kelly, J. D., and Hedengren, J. D. (2020). Benchmark temperature microcontroller for process dynamics and control. *Computers & Chemical Engineering*, 135:106736.
- Pataro, I. M., Gil, J. D., da Costa, M. V. A., Roca, L., Guzmán, J. L., and Berenguel, M. (2023). Improving temperature tracking control for solar collector fields based on reference feedforward. *IEEE Transactions on Control Systems Technology*, 31(6):2596–2607.
- Proaño, P., Capito, L., Rosales, A., and Camacho, O. (2017). A dynamical sliding mode control approach for long deadtime systems. In *2017 4th International Conference on Control, Decision and Information Technologies (CoDIT)*, pages 0108–0113. IEEE.
- Rojas, R., García-Gabín, W., and Camacho, O. (2005). On sliding-mode control for inverse response processes. *IFAC Proceedings Volumes*, 38(1):525–530.
- Rossiter, J. A., Cassandras, C. G., Hespanha, J., Dormido, S., de la Torre, L., Ranade, G., Visioli, A., Hedengren, J., Murray, R. M., Antsaklis, P., et al. (2023). Control education for societal-scale challenges: A community roadmap. *Annual Reviews in Control*.
- Salinas, L. R., Santiago, D., Slawiński, E., Mut, V. A., Chavez, D., Leica, P., and Camacho, O. (2018). P+d plus sliding mode control for bilateral teleoperation of a mobile robot. *International Journal of Control, Automation and Systems*, 16(4):1927–1937.
- Sardella, M. F., Serrano, E., Camacho, O., and Scaglia, G. (2021). Improvement of linear algebra controllers using sliding surface concepts: applications to chemical processes. *IEEE Latin America Transactions*, 19(8):1299–1306.
- Seborg, D. E., Edgar, T. F., Mellichamp, D. A., and Doyle III, F. J. (2016). *Process dynamics and control*. John Wiley & Sons.
- Sira, H., Ramirez, M. Z., and Ahmed, S. (1994). Dynamical sliding mode control approach for vertical flight regulation in helicopter. In *IEEE Proc-Control Theory App*, volume 141, pages 19–24.
- Utkin, V., Poznyak, A., Orlov, Y. V., and Polyakov, A. (2020). *Road map for sliding mode control design*. Springer.
- Vegi, S. and Shastri, Y. (2017). Optimal control of dilute acid pretreatment and enzymatic hydrolysis for processing lignocellulosic feedstock. *Journal of Process Control*, 56:100–111.